

# Pressure-Sensitive Paint Measurements on the NASA Common Research Model in the NASA 11-ft Transonic Wind Tunnel

James H. Bell  
NASA Ames Research Center  
Mountain View, CA

**Abstract:** The luminescence lifetime technique was used to make pressure-sensitive paint (PSP) measurements on a 2.7% Common Research Model in the NASA Ames 11ft Transonic Wind Tunnel. PSP data were obtained on the upper and lower surfaces of the wing and horizontal tail, as well as one side of the fuselage. Data were taken for several model attitudes of interest at Mach numbers between 0.70 and 0.87. Image data were mapped onto a three-dimensional surface grid suitable both for comparison with CFD and for integration of pressures to determine loads. Luminescence lifetime measurements were made using strobed LED (light-emitting diode) lamps to illuminate the PSP and fast-framing interline transfer cameras to acquire the PSP emission.

## Nomenclature

$b$	Wing span
$c$	Wing mean aerodynamic chord
$C$	Integrated light intensity falling on a pixel
$C_p$	Pressure coefficient
$I$	Luminescence intensity
$I_0$	Initial luminescence intensity
$M$	Mach number
$R$	Luminescence intensity ratio
$S$	Wing area
$t$	Time
$\alpha$	Angle of attack
$\eta$	Normalized spanwise coordinate
$\sigma$	Standard deviation
$\tau$	Luminescence lifetime

## I. INTRODUCTION

### A. The NASA Common Research Model

NASA and the aerospace community have long recognized the value of common wind tunnel models dedicated to research purposes. A common research model is one intended for use by a wide variety of research projects in a large number of facilities. Ideally a common research model should be applicable to the study of a variety of problems of current interest. Furthermore the model should be suitable for as wide a variety of wind tunnels and instrumentation techniques as possible. Finally the model should be as free as possible from concerns about intellectual property and proprietary information, to maximize the number of programs able to benefit from the data it produces.

The present NASA Common Research Model<sup>1</sup> (CRM), shown in figure 1, is a 2.7% model of a generic commercial transport. The model has several features designed to boost its utility for studying the aerodynamics of commercial transports. The primary feature is a modern wing design. The model can also be fitted with flow-through nacelles as well as horizontal stabilizers. The stabilizer incidence angle can be adjusted via a model change. The model is also mounted using a sting which enters through the vertical stabilizer, allowing it to faithfully reproduce the tail cone contours of modern transport aircraft.



Figure 1. Common Research Model (unpainted) in test section of NASA 11ft wind tunnel.

The CRM is designed to withstand the extreme loads and temperature conditions of cryogenic wind tunnels, and is sized appropriately for most large transonic wind tunnels. It is extensively instrumented with pressure taps on the wings, and was designed to be compatible with optical instrumentation techniques.

The inaugural tests of the CRM were conducted in the National Transonic Facility at the NASA Langley Research Center and the 11ft transonic leg of the Unitary Plan Wind Tunnel at the NASA Ames Research Center. The test in the National Transonic Facility<sup>2</sup> (NTF) focused on aero performance at flight Reynolds numbers, and obtained flow diagnostic information using the NTF's recently-deployed PSP

system. The test in the 11ft, in addition to aero performance studies, also included optical diagnostic techniques made possible by the test section's relatively generous optical access. The optical techniques used in the CRM test were Particle Image Velocimetry (PIV), Fringe Imaging Skin Friction (FISF), and Pressure Sensitive Paint (PSP). The deployment of and results from the PSP technique is the subject of the present paper.

### B. Theory of the Luminescence Lifetime Technique for Pressure-Sensitive Paint Measurements

Pressure-sensitive paint measurement systems exploit the sensitivity of certain luminescent materials to air pressure due to the phenomenon of oxygen quenching. In a typical luminescent molecule, excitation by capture of a high energy photon is followed, after a random time delay, by emission of a lower energy photon. When a large population of luminescent molecules is simultaneously excited (perhaps with a flash lamp) and subsequently allowed to decay, the time required for light intensity to drop by a factor of  $e$  denotes the "luminescence lifetime." It represents the characteristic time the molecules spend in an excited state. In oxygen-quenched materials, the excited luminescent molecule can also react with a nearby oxygen molecule, losing its excitation energy without emitting a photon. The longer a molecule remains in an excited state the greater the chance for oxygen quenching. Thus, increased oxygen concentration reduces the luminescence lifetime of an oxygen-quenched material. In the limiting case of steady state (as opposed to pulsed) excitation, the effect of oxygen is to make the luminescence dimmer. The oxygen concentration in an oxygen-permeable surface layer is proportional to the air pressure, so a luminophor suspended in such a layer becomes a pressure sensor.

Luminescence lifetimes of PSPs range from 0.3 to 50  $\mu\text{sec}$ <sup>3,4</sup>, which is much faster than most imaging systems can resolve. Accordingly, most early PSP systems used continuous excitation and measured time-averaged luminescence<sup>5</sup>. Since luminescence also depends on extraneous factors such as excitation intensity and (for paints) paint thickness, it was necessary to compare two images; a wind-on image taken under test conditions and a wind-off image taken at a known constant reference pressure. The pixel-to-pixel ratio of the two images is proportional to the luminescence lifetime, and thus to pressure. This is generally known as the "radiometric" approach. The requirement for a separate wind-off image leads to several complications. For example, between the time the wind-on and wind-off images are taken, the model may move slightly, its temperature may change, illumination may change, and the paint may photodegrade. All these effects will be erroneously sensed as a pressure change. Furthermore, in large facilities in particular, it may be difficult to arrange for reference images be taken in a timely manner.

An imaging system which makes a measurement of lifetime is very desirable, since a wind-off image is not required. One way to do this is by means of a camera with a very fast shutter. Fig. 2 generically shows the response of PSP to a single

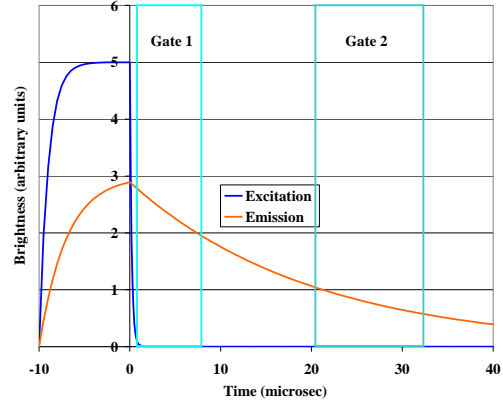


Figure 2. Diagram showing timing of excitation and emission light curves, including gates during which camera is exposed (green boxes).

excitation pulse. The excitation, which is nominally a square wave, is shown as a blue line; the resulting emission is shown in red. During the excitation pulse, emitted intensity increases with time; for a sufficiently long excitation pulse it would saturate at some steady state brightness. If the excitation pulse ends at time 0, and the emitted intensity at that time is  $I_0$ , the emission then decays exponentially, following the relation

$$I = I_0 e^{-t/\tau}, \quad (1)$$

where  $I$  is the emitted intensity,  $t$  is time, and  $\tau$  is the lifetime, which is to be determined. If the camera shutter is opened at time  $t_1$  and closed at time  $t_1 + \Delta t_1$ , the amount of light falling on a pixel will be

$$C_1 = \int_{t_1}^{t_1 + \Delta t_1} I_0 e^{-t/\tau} dt = I_0 \tau e^{-t_1/\tau} [1 - e^{-\Delta t_1/\tau}]. \quad (2)$$

In general,  $I_0$  is not known. However, if the variation in excitation from one pulse to the next is negligible, a second image can be obtained following another pulse at a different gate time,  $t_2$  and the unknown quantities can be factored out as shown below.

$$R = C_2 / C_1 = e^{(t_1 - t_2)/\tau} \frac{[1 - e^{-\Delta t_2/\tau}]}{[1 - e^{-\Delta t_1/\tau}]} \quad (3)$$

By inverting (3), it is possible to determine  $\tau$ , which is related to pressure via the well-known Stern-Volmer equation<sup>6</sup>. This is known as the "lifetime" method. For any two images, the one taken at a greater delay after the excitation pulse should show more pressure effect, since the more delayed the luminescence, the greater the chance for quenching interaction to occur. Notice that if  $\Delta t_1 = \Delta t_2$ , then it is very easy to invert (3) and find  $\tau = (t_1 - t_2) / \log(C_2/C_1)$ . However, the sensitivity of the image ratio  $C_2/C_1$  to pressure can be optimized by adjusting the gate timings<sup>7,8</sup>, and so in practice the gate durations may not be equal.

In practical applications, it has been noted that luminescence lifetime may vary from point to point on a PSP-coated surface even when pressure is constant across the surface<sup>6</sup>. Because the point-to-point lifetime variation is constant with time, this error term can be eliminated by taking data both at the test condition and at a constant pressure reference "wind-off" condition. The reference data provide a map of the point-to-point lifetime

variations which can be used to correct the test image. In contrast to the wind-off reference used for conventional PSP measurements, the wind-off lifetime measurement is much less sensitive to changes in model illumination and position, and is thus much easier to obtain.

### C. Survey of Pressure-Sensitive Paint Measurements using the Luminescence Lifetime Technique

Lifetime PSP measurements date back to nearly the beginning of the PSP method itself, when Radchenko<sup>9</sup> used the lifetime method to measure pressures on a cone-cylinder at supersonic Mach numbers. Radchenko used the technique because his paint suffered from such a high photodegradation rate that conventional “wind-off/wind-on” measurements were impossible. Subsequently, the lifetime technique languished. An attempt by Levy<sup>10</sup> to revive the technique illustrates the reasons why. Levy found that the microsecond-range shutter speeds needed to capture the paint’s luminescence decay could only be achieved with an image intensifier. But the intensifier degraded spatial resolution and added significant random

noise. The resultant images had poorer quality than those produced by conventional PSP techniques even when longer data acquisition time was used for signal averaging. This negated one of the method’s perceived advantages – lower data acquisition time due to the lack of need for wind-off reference measurements. Moreover, the lifetime method suffered from additional complexity due to the intensifier, its high voltage power supply, and the exotic flashlamps needed to produce sufficiently short illumination pulses. It seemed that all the advantages of the lifetime technique could be achieved with less trouble through biluminophore paints.

The lifetime method fared better in non-imaging applications<sup>11</sup>, where a pulsed laser could be used for spot illumination and a high speed photodiode to measure the decay curve of the paint luminescence. Arguably the most advanced non-imaging system is that developed by Davies<sup>12</sup>, which can extract both pressure and temperature from the higher order shape of the decay curve and measure fluctuating pressures up to several kHz. Although non-imaging PSP systems have been developed with sophisticated beam-pointing equipment to map

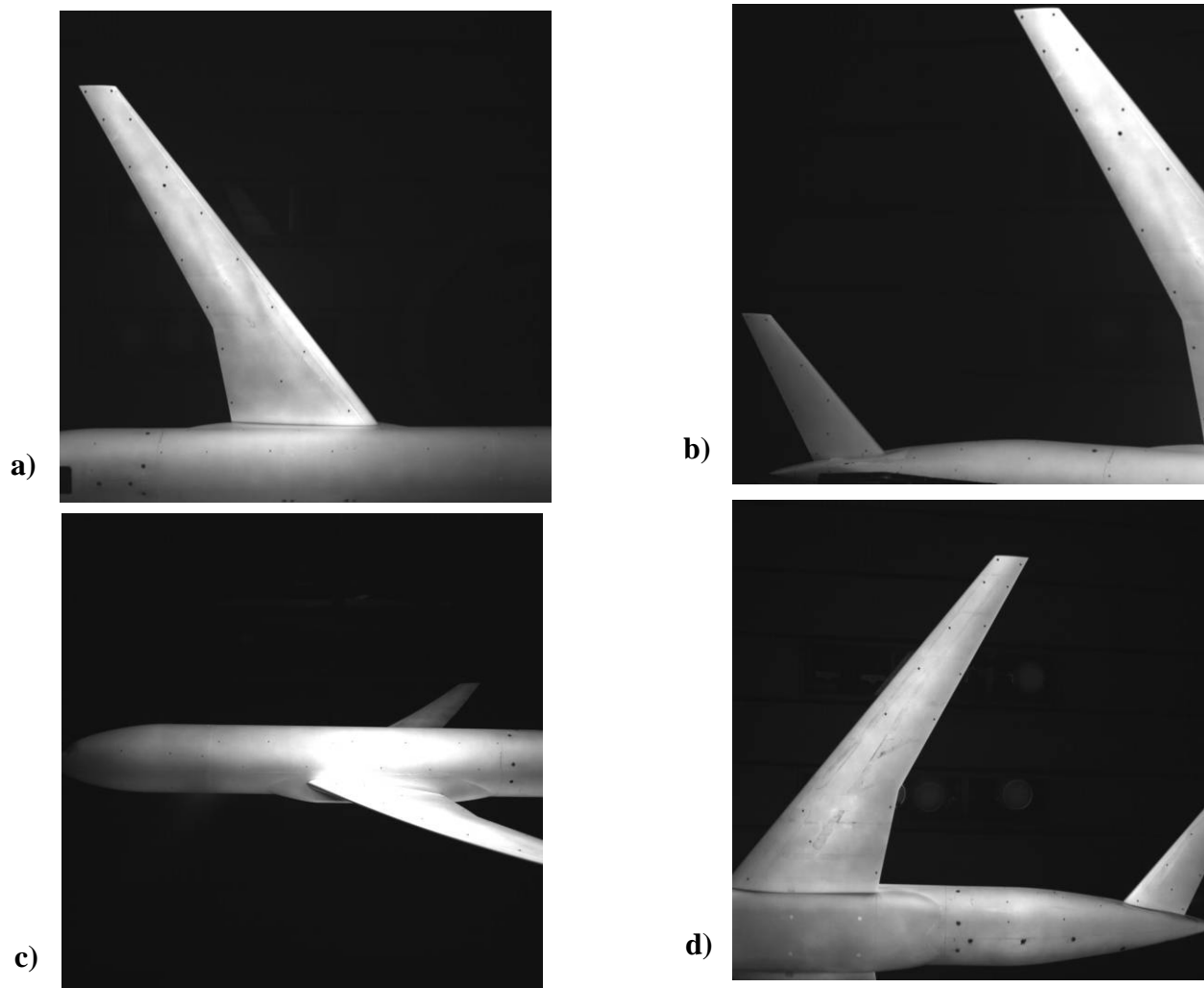


Figure 3 Typical raw PSP images of CRM model: a) camera 1 viewing left wing and fuselage upper surface, b) camera 2 viewing upper horizontal tail and aft fuselage, c) camera 3 viewing left wing root obliquely, and d) camera 4 viewing lower surface of wing, aft fuselage, and horizontal tail.

out surface pressures, they still are unable to match the spatial resolution of imaging systems, however.

The development of imaging lifetime systems was revived in the late 1990's by several researchers. Holmes<sup>13</sup> demonstrated a lifetime system which used a fast framing interline transfer camera instead of an intensified camera. Interline transfer allowed the camera to be shuttered with significantly less noise than an image intensifier. Bright blue and UV LED (Ultra-Violet Light Emitting Diode) lamps which could be easily driven at the desired pulse rates began to become available. At the same time, it had been found that biluminophor paints could only reduce, and not eliminate, the requirement for wind-off images. The lifetime method held out the possibility of a complete elimination of this requirement. As a result, the lifetime method was strongly advocated by engineers at Lockheed Martin who saw the operational complexity of existing PSP systems as a major barrier to their use in large wind tunnels<sup>14, 15</sup>.

Responding to these developments, engineers at AEDC constructed an institutional PSP system for the 16T transonic wind tunnel<sup>16</sup>. The original system used intensified CCD (Charge-Coupled Device) cameras to achieve the required fast-shuttering capability, but the system has now been upgraded with fast framing interline transfer cameras. The luminescence lifetime approach with fast framing interline transfer cameras has become the standard approach used in large facilities at AEDC and NASA Ames, and is in common use at NASA Glenn and NASA Langley as well

## II. EQUIPMENT AND EXPERIMENTAL PROCEDURE

### A. 2.7% Common Research Model

The model provided for this test was the NASA Common Research Model, which is a 2.7% scale model of a generic commercial transport. The CRM, shown in figure 1, is designed for a cruise Mach number of  $M=0.85$  and a lift coefficient of  $C_L=0.5$ . The aspect ratio is 9.0, the leading edge sweep angle is  $35^\circ$ , the wing reference area is  $S=3.01 \text{ ft}^2$ , the wing span is  $b=62.46 \text{ in}$ , and the mean aerodynamic chord is  $c=7.45 \text{ in}$ . The CRM has removable horizontal stabilizers and flow-through nacelles. The model is supported by a blade mount entering the dorsal side of the rear fuselage. Three sets of horizontal stabilizers have been produced, representing the stabilizer at  $-2^\circ$ ,  $0^\circ$ , and  $+2^\circ$  to the nominal angle of incidence. Thus the CRM can be tested several configurations: the wing/body (WB) alone, wing/body/nacelle/pylon (WBNP), wing/body/tail= $0^\circ$  (WBT0), wing/body/tail= $+2^\circ$  (WBT+2), wing/body/tail= $-2^\circ$  (WBT-2). The WBT configurations can be tested with nacelle/pylons attached as well. For the present test only the WBT, WBT0, and WBT+2 configurations were tested with PSP. The CRM wing is constructed from Vascomax, while the fuselage and horizontal stabilizers are constructed from 17-4 PH steel.

The model is extensively instrumented with conventional pressure and force instrumentation. The wing has a total of 303 pressure taps arranged in 9 chordwise rows at  $\eta = 0.131, 0.201,$

$0.283, 0.397, 0.502, 0.603, 0.727, 0.846,$  and  $0.950$ . Upper surface taps are located on the left wing while lower-surface taps are on the right wing. There are six pressure taps on the flow-through nacelles. A single high-speed pressure transducer is installed on the upper surface to measure shock oscillation. In addition to the balance a wing-root bending moment gauge

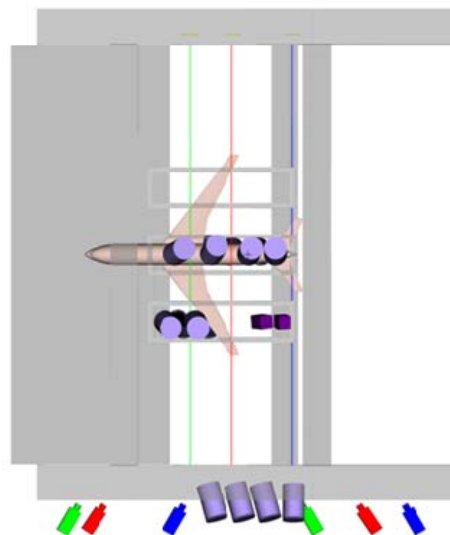


Figure 4a. Synthetic top view of CRM in test section produced by Vinci software, showing positions of lamps (grey cylinders) and cameras (colored boxes).

is also installed. Trip dots were installed on the model nose, wing, and horizontal tail as described in reference 2. Wing trip dots were installed at 10% chord.

For the present test the model was installed using a strut which included an active damper. The active damper used 12 piezo-electric actuators to minimize model vibration in the flow. This allowed the model to be tested at higher angles of attack and also made the model a more stable platform for optical sensors, including PSP.

### B. 11x11ft Transonic Wind Tunnel

The 11x11ft Transonic Wind Tunnel (TWT) is part of the Unitary Plan Wind Tunnel (UPWT) complex at the NASA Ames Research Center. The wind tunnel is driven by a 3-stage compressor turned by a 176 MW electric motor system. A general description of the facility can be found at <http://windtunnels.arc.nasa.gov/>, and the facility is additionally described by Amaya & Kmak<sup>17</sup> as well as Amaya & Boone<sup>18</sup>, from which the present description is taken. Readers seeking more detailed information are referred to the NASA Ames UPWT test planning guide<sup>19</sup>.

The 11x11-Foot TWT is a closed-circuit, variable-pressure, continuous operation wind tunnel. Subsonic Mach number control is achieved with a combination of compressor drive speed control and variable-camber guide vanes at the compressor inlet. Supersonic Mach number control additionally involves setting the flexible wall nozzle to achieve



the proper area ratio. The tunnel can be operated over a Mach number range of 0.2 to 1.45, and at total pressures of up to 32 psia. Operating air temperatures can range from 80° F to 150° F, but the facility is normally operated at temperatures around 100° F. The wind tunnel has reached a maximum Reynolds number capability of  $9.6 \times 10^6/\text{ft}$  at  $M=1.2$ . Over the transonic range ( $0.7 \leq M \leq 1.4$ ) the tunnel can reach a Reynolds number of  $8.0 \times 10^6/\text{ft}$ . The test section is 11-by 11-feet in cross section and 22 feet in length. Slots in all four walls run the full length of the test section. The slots contain baffles that provide a 6-percent porosity into the plenum chamber. Windows located in all four of the test section walls between the slots provide optical access to the test section.

The primary model support is a knuckle-sleeve assembly mounted on a traversing strut located aft of the test section. The knuckle-sleeve can position the model at any attitude circumscribed by a 15° half-angle cone, while the strut is traversed to maintain the model as nearly as possible in the center of the test section.

### C. Camera and Lamp System

Four Roper Scientific CoolSNAP K4 cameras were used for this test. The cameras are equipped with Kodak KAI4040M CCD sensors, which have  $2048 \times 2048$  array of  $7.4 \times 7.4 \mu\text{m}$  pixels. Pixels are read out with a 12 bit digitizer at a rate of 10 MHz. Each pixel has a full well capacity of about 40,000 electrons. The CCDs use interline transfer for readout and have a fast-framing capability, whereby charge can be repeatedly shifted from each pixel to an adjacent storage well. This capability allows the camera to take several thousand short “gates” at a well-defined delay time after a light pulse, accumulating the photoelectrons collected in each gate before readout. With the current camera and CCD, individual gates as short as 1  $\mu\text{sec}$  are possible. The maximum gate repetition rate is limited to roughly 40 kHz by the 25  $\mu\text{sec}$  gate delay of the Kodak CCD.

All four cameras were equipped with 18-36mm/f2.8 zoom lenses. Bandpass interference filters with a pass frequency of 650 nm and a bandpass of  $\pm 20$  nm were placed in front of each lens. The filters were special-ordered from Andover Co and have a peak transmission of 70% at 650 nm.

The PSP-coated model surface was illuminated by fourteen blue LED lamps. Each lamp consists of roughly 22 high brightness LEDs mounted on a 10.2cm (4”) diameter disk. The lamps’ peak output wavelength is 408 nm. A bandpass interference filter is placed in front of the lamp to diffuse the individual LED outputs and to minimize light output at the paint emission frequency of 650 nm. The lamps can be adjusted for either pulsed or continuous operation. In pulsed mode, the lamps are limited by their rise time of approximately 200 nsec, fall time of approximately 1  $\mu\text{sec}$ , and maximum duty cycle of 5%. The LEDs are driven at approximately  $10 \times$  their rated peak continuous current to maximize brightness. The lamps are manufactured by Innovative Scientific Solutions, Inc.

Both cameras and lamps are controlled by TTL timing signals. In the present test these were generated by a Stanford Research Systems DDG535 digital delay generator which was in turn controlled by the data acquisition software.

### D. Camera and Lamp Positioning

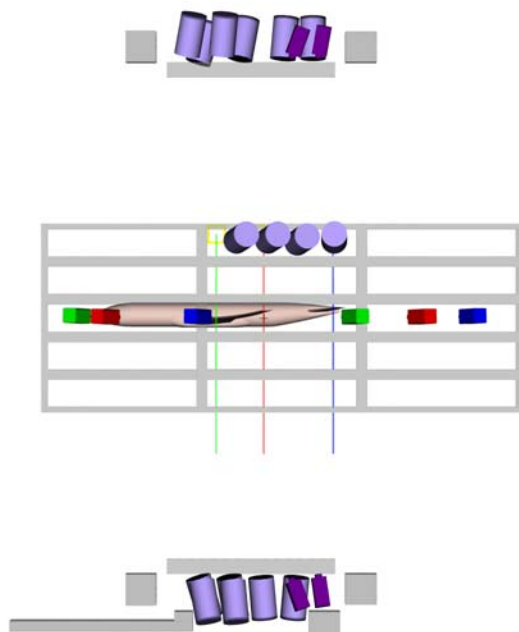


Figure 4b. Synthetic side view of CRM in test section produced by Vinci software. Modeling of tunnel walls is limited to window frames and structures most likely to occlude cameras and lamps.

Optical access within the 11ft test section is sufficient to view the entire model. Actual PSP coverage for the CRM test was determined by several factors – the required surface data, the desire to obtain high resolution in critical areas, the higher complexity of additional PSP cameras, and the need to share window space with the other optical instruments. Typical views of the model from each camera are shown in figure 3. Since the test was run with the model at zero sideslip, the flow over the left and right sides was considered to be symmetrical. It was therefore decided to position cameras so as to view the left side of the model only. Two cameras were used to view the upper surface of the left wing and horizontal stabilizer, while a third was used to view both the wing and horizontal stabilizer from below. (It was desired to have higher resolution of the wing upper surface than the lower surface.) A fourth camera viewed the wing root and forward fuselage from the side. Although viewing the entire model would have allowed integrating the PSP data to obtain forces, by confining the PSP equipment to the top, bottom, and left side, the right side of the test section was freed up for PIV equipment.

Camera and lamp positions were optimized by L. Kushner using the “Vinci” visualization software<sup>20, 21</sup> developed by E. Schairer at NASA Ames. The software allowed camera and lamp pointing angles and camera zoom settings to be estimated

ahead of time in order to speed installation. In addition the software allowed lamp placement to be optimized so as to achieve even illumination of the model – this is useful to ensure that the PSP signal-to-noise level is consistent across the image. Figure 4 shows typical Vinci output, demonstrating the modeling of cameras, lamps, the wind tunnel model, and key wind tunnel structures most likely to interfere with camera and lamp placement. By pre-visualization all the camera and lamp equipment in the test section, it was possible to ensure that the PSP equipment would not interfere with the PIV installation, which had to occupy both sides of the test section..

#### E. Pressure-Sensitive Paint

PSP was applied to the model in three distinct layers. The top, or active, layer consists of the actual pressure-sensitive luminescent coating. The middle layer, or basecoat, acts to chemically isolate the active layer from the model and to provide a low contrast white surface. The bottom, or screen, layer, promotes adhesion of the basecoat while further providing a low contrast white surface. The active layer was FIB-7 topcoat which uses platinum tetra (pentafluoro- phenyl) porphine (PtTFPP) as the probe molecule and FIB-7 as the oxygen-permeable polymer binder. PtTFPP is commonly used as a pressure sensor because of its high quantum efficiency and low inherent temperature sensitivity. FIB-7 is a fluorinated copolymer designed for use with PtTFPP. The properties of this combination have been described in detail by Ponomarev



Figure 5. Application of PSP basecoat in model prep room. Model can be rolled to provide access to all surfaces for painting. Fans at left provide ventilation.

& Gouterman<sup>22</sup>. For lifetime PSP measurements, PtTFPP has the additional advantage of a relatively long luminescence lifetime (vacuum lifetime  $\sim 80$   $\mu\text{sec}$  at room temperature). The basecoat consisted of FIB-7 with titanium dioxide added as a scatterer. Both these paints are manufactured by Innovative Scientific Solutions, Inc., of Dayton, Ohio. The screen layer consisted of a commercial white epoxy paint (Krylon Hi-Heat). The use of a screen layer tends to increase the temperature-sensitivity of the PSP, but the screen layer has been found to

significantly improve the adhesion of the FIB-7 basecoat to highly polished steel surfaces..

PSP was applied to the CRM model in a prep room just prior to installation of the model in the wind tunnel. This approach has several advantages relative to application of PSP in the test section. It allows more time for paint application which contributes to a higher quality coating and avoids the wind tunnel occupancy cost that would result from painting in the test section. However it makes the PSP coat vulnerable to damage during installation, especially if the model must be opened to install balance calibration equipment or to diagnose instrumentation problems. Fortunately the design of the CRM model minimizes the impacts of such operations and makes PSP application outside of the test section a practical option.

The model was prepared by thoroughly cleaning the surface with detergent followed by acetone, and by masking off those areas which were not to be painted. The horizontal stabilizers were not attached to the model at this point, but were painted simultaneously with the rest of the model. The screen layer was applied in 3-4 light coats and allowed to dry for roughly 45 minutes. The basecoat was applied very dry, in about 15 light passes with a spray gun. This coat was allowed to dry for 30 minutes and then sanded with 9 micron buffing pads to produce a surface smooth to  $<20$  micro-inches. The active layer was then applied. This was also done very dry, in about 15 light passes with a spray gun. Considerable care was taken to maintain a consistent paint thickness over the entire model by equalizing the number of passes, distance from the spray gun to the model, and the speed of advance of the spray gun. The screen layer and basecoat were applied to the entire model, while the active layer was applied only to the left-side regions viewed by the cameras. This was done to maintain a consistent roughness over the entire model surface.

Once the model was painted the coating was annealed by placing the model in an insulated box and raising the temperature to  $150^{\circ}\text{F}$  for four hours. This process raises the PSP above its glass transition temperature and reduces the temperature sensitivity of the paint luminescence output.

Following the conclusion of the PSP portion of the test the paint was removed using rags soaked with acetone.

#### F. Photogrammetry Targets

Black target dots were marked on the model surface to serve as calibration points for photogrammetry, which was used to accurately map image data onto a model surface grid. Normally targets are drawn on the model with a permanent marker and their positions are measured with a coordinate measuring arm. For the CRM test, though, a new procedure was employed. During test planning it was noted that the FISF technique, scheduled to be used after PSP would also require photogrammetry targets. However it would be impossible to re-use the normal PSP targets because these would be removed along with the paint while preparing the model surface for FISF. In addition, if it became necessary to remove and re-apply the PSP due to handling damage, the targets would have to be re-applied and re-measured as well.

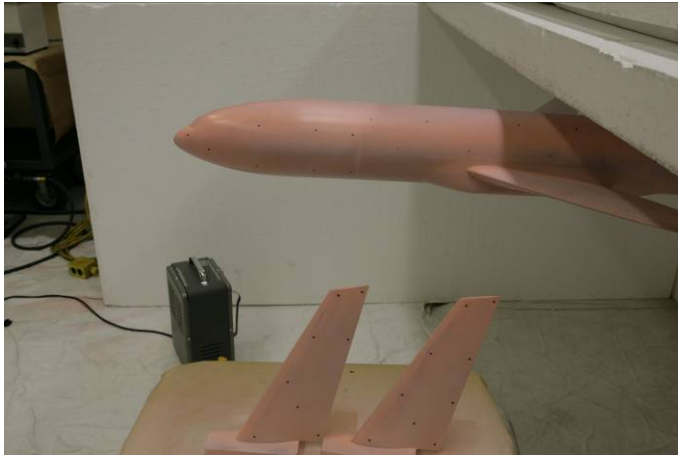


Figure 6. Model being placed in insulated enclosure for annealing. Horizontal stabilizers (painted separately) are visible at bottom. Photogrammetry targets can be seen on model and stabilizers,

The alternate approach proposed was to mark the metal surface of the model directly with an acid-etch technique or gun-bluing solution. The marks thus produced would be unaffected by the acetone used to remove the paint and would be of sufficient contrast to show through the PSP-coated surface. G. Zilliac developed an acid etch system which was successfully applied to the wing and horizontal stabilizers. However the acid-etch solution did not mark the fuselage effectively. (The wing and stabilizers were Vascomax while the fuselage was 17-4 PH steel.) Gun-bluing solution was used instead to mark the fuselage. The target marks consisted of 6mm ( $\frac{1}{4}$ " diameter disks and their positions were measured in the standard fashion with a coordinate measuring arm. The arm has a quoted accuracy of 0.13mm (0.005"), but measurements of the target positions had a repeatability of 0.8mm (0.03"), due primarily to uncertainty in touching the exact center of the target with the probe tip. Following PSP application the targets were visible but with low contrast. Each target was overdrawn with a permanent marker to improve contrast, with great care being taken to ensure that the overdrawing did not shift the apparent position of the target. No degradation of the photogrammetric accuracy was noted and the targets were successfully re-used for FISF.

#### G. Data Acquisition Procedure

The CRM test plan called for data acquisition on three model configurations; one without horizontal stabilizers and two with stabilizers at different angles to the fuselage. For each configuration data were taken at three Mach numbers and nine different angles of attack. The range of Mach, Reynolds number, and  $\alpha$  are given in table 1 for each model configuration. In addition to "wind-on" images with the tunnel running, "wind-off" images were also taken as part of the camera checkout and data reduction process. For each configuration, three sets of wind-off images were taken prior to

starting the tunnel to study the response of the PSP to static pressure variations. Images were taken at three different static pressures: 20, 25, and 28 psi. At each static pressure images were taken over the same range of pitch angles as the wind-on runs. An additional wind-off run was taken over the full range of pitch angles after the completion of the wind-on run series for each configuration..

Table 1. Model configuration and wind tunnel conditions at which PSP data were taken.

Configuration	Mach	Re/ft	$\alpha$ ( $^{\circ}$ )
WB	0.7, 0.85, 0.87	$8.06 \times 10^6$	0, 0.5, 1.0,
WBT+2	0.7, 0.85, 0.87	$8.06 \times 10^6$	1.5, 2.0, 2.5,
WBT0	0.7, 0.85, 0.87	$8.06 \times 10^6$	3.0, 3.5, 4.0

Data were taken in lifetime mode only. Each lifetime image was formed by summing (accumulating) 2500 to 3000 individual gates. The number of accumulations varied with test condition and was chosen to produce final images of high brightness without saturating any part of the image. The number of accumulations was chosen at the beginning of each run and was not changed during the run.

Camera noise rises with number of accumulations; to minimize accumulations, the paint's emission over a single accumulation should be as high as possible. The LED lamp brightness per flash increases linearly with flash duration. but the induced paint emission reaches a plateau for flash durations much longer than the luminescence lifetime, as shown in fig. 2. Thus flash duration should be roughly equal to the paint's luminescence lifetime. For the current test, a 20  $\mu$ sec flash duration was chosen as being roughly equal to the paint's expected lifetime at the test conditions. Total cycle time for the flash lamp was therefore fixed at 400  $\mu$ sec by the lamps' maximum duty cycle, implying a flash rate of 2500 Hz. At this flash rate, a single image with 3000 accumulations requires 1.2 seconds exposure time.

Two data images were taken at each test condition. One image (gate 1) was taken with a delay of 0  $\mu$ sec relative to the flash, while the second (gate 2) was taken with a delay of 23  $\mu$ sec. Thus gate 1 was taken during the flash while gate 2 was delayed until 3  $\mu$ sec after the flash ended – allowing time for the fall-off curve of the LEDs. Prior to taking data images, a single accumulation at zero delay was read out in order to clear the CCD of accumulated charge. (Operation in lifetime mode disables the normal pre-exposure clear process for this camera.) The total time to take all images, including readout and storage times, was five to six seconds. At the end of each run "dark" images were taken with the lamps turned off. These images provide data on the bias level of charge present on the CCD with no illumination. Dark images were obtained at the same number of accumulations as the data images.

PSP data acquisition was synchronized with wind tunnel operations through a network utility available at the Unitary Wind Tunnel. The utility allowed the wind tunnel to broadcast to the PSP system when the wind tunnel was "on condition" and to transmit the assigned run and test point (sequence)



number to the PSP system. Similarly, the PSP system could advise the wind tunnel when it was finished taking data, freeing the tunnel to move on to the next test condition. Data from the pressure taps were not transferred to the PSP system immediately, but were made available for post-processing.

The blue LED lamps were operated continuously during the PSP measurement campaign, and were the only source of illumination in the wind tunnel. All other light sources were turned off and all windows were covered with blackout curtains. The light provided by the LED lamps was deemed acceptable for model watching and safety purposes.

#### H. Data Reduction Procedure

The data reduction procedure is separated into the following steps; processing of raw images into intensity ratio images, conversion of intensity ratio data to pressure data, and mapping onto the model surface grid. All data reduction operations were done with the “Green Boot” PSP data reduction software.

*Image processing:* Raw images were first corrected for bias in the CCD measurement by subtracting the post-run dark image. After dark subtraction pixels below a threshold value (typically 100-300 counts) were set to zero in order to remove clutter from the images.

The photogrammetry target dots painted on the model were

then located in all gate 1 images. The coarse locations of targets in an initial reference image were supplied manually. This solution was then refined and propagated to all other images from the same camera using automated target-finding software, using a centroiding algorithm which has previously demonstrated an accuracy of 0.05 pixels in test cases. (Target locations are the same in gate 1 and gate 2 images since there is negligible model motion between images. Target-finding is more accurate in the brighter gate 1 images.) The targets in each image were related to the target locations on the model by means of a Direct Linear Transform algorithm. This allows a general mapping to be determined between model and image coordinates. The accuracy of the photogrammetry was estimated at approximately 1.5 pixels, or 0.8 mm (0.03”), based on the rms difference between the predicted and measured locations of the targets in the images. This is within the known accuracies of the target measurements in both model and image space.

*Image ratioing:* Next, intensity ratio images were formed by taking the pixel-by-pixel ratio of the gate 1 image at each test condition divided by the gate 2 image. For extremely simple cases, as shown by (3), the intensity ratio is the logarithm of the pressure ratio. The intensity ratio image is a useful intermediate step and gives a good qualitative indication of the

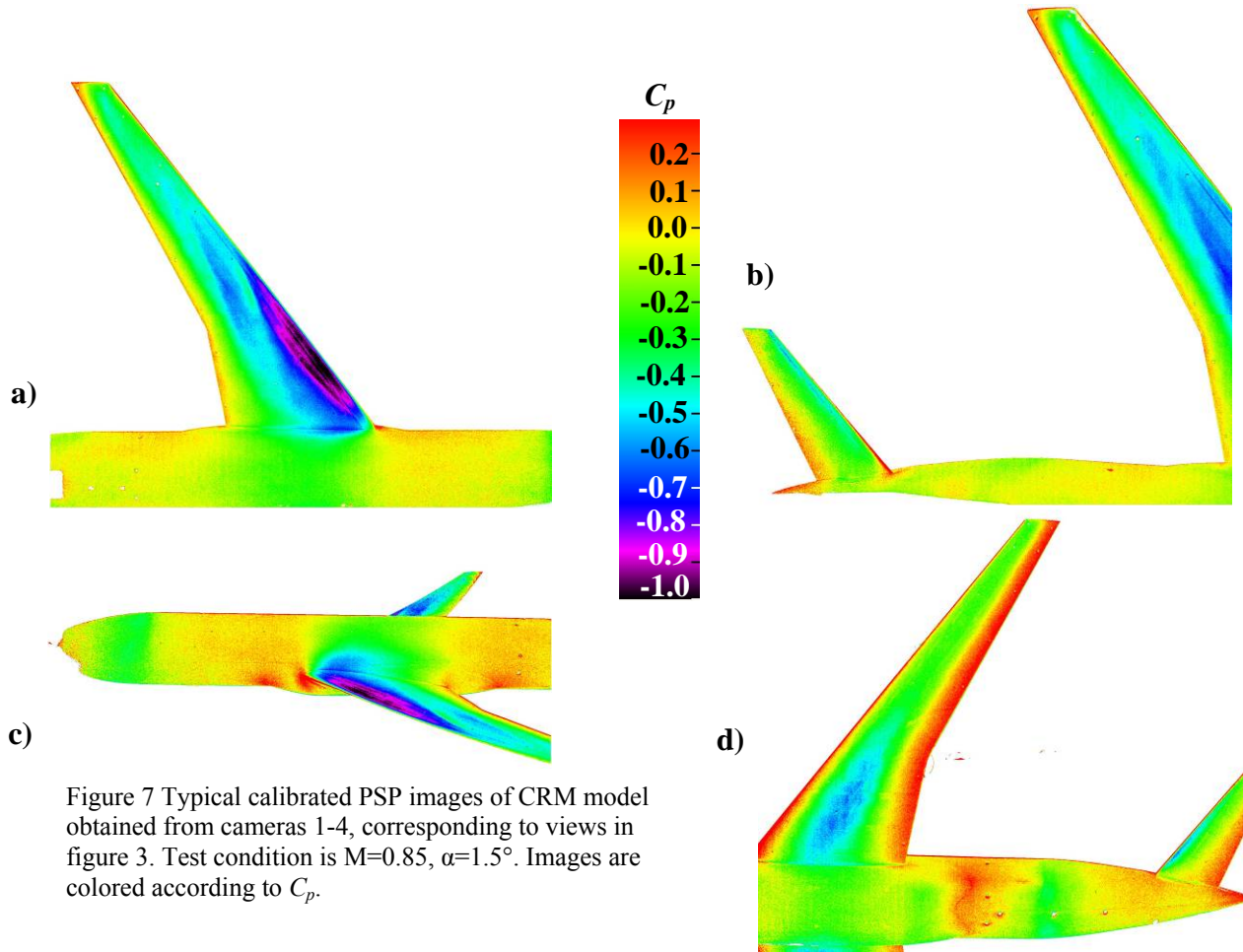


Figure 7 Typical calibrated PSP images of CRM model obtained from cameras 1-4, corresponding to views in figure 3. Test condition is  $M=0.85$ ,  $\alpha=1.5^\circ$ . Images are colored according to  $C_p$ .



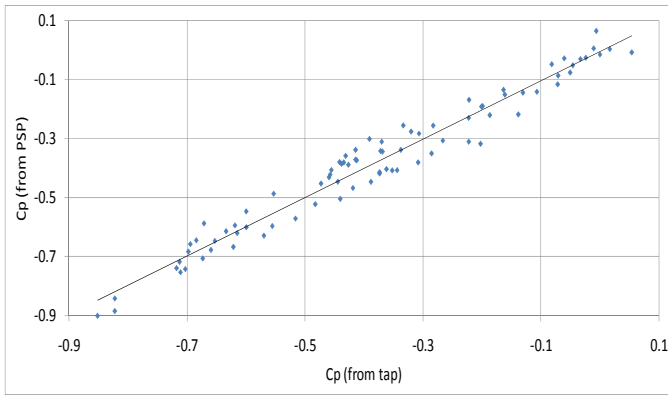


Figure 8 Typical scatter plot of PSP vs tap data after *in situ* calibration. (Data shown for Run 57 Seq 4,  $M = 0.85$ ,  $\alpha = 1.5^\circ$ .)  $1-\sigma$  Scatter at this condition is  $0.046$  in  $C_n$  units.

pressure field. In addition, the ratioing procedure factors out any pixel-to-pixel variation in gain of the CCD, which can be a significant source of error. The intensity ratio images were further ratioed by dividing each by a “wind-off” intensity ratio image taken with the tunnel compressor off immediately after each run series. Each intensity ratio image was matched with a reference image taken at the same angle of attack. Since the model was slightly deformed by airloads, the test image was warped, or registered, to match the wind-off image. This was done using a polynomial transform which matched the locations of the targets in each image.

*Image calibration:* All images were calibrated *in situ* by

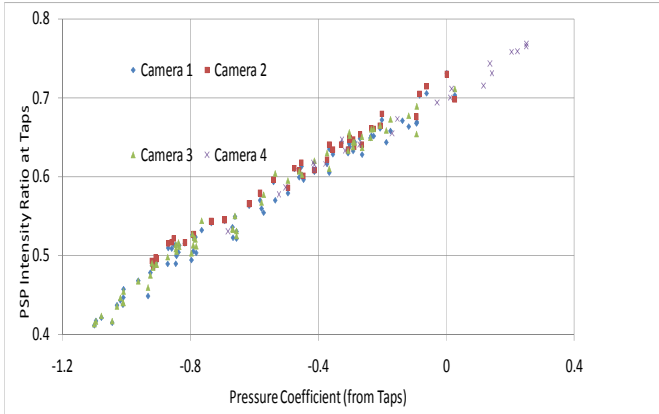


Figure 9 Scatter plot of PSP intensity ratio (prior to calibration) vs pressure taps showing all four cameras separately. (Data shown for Run 36 Seq 9,  $M = 0.87$ ,  $\alpha = 4.0^\circ$ .)  $1-\sigma$  Scatter at this condition is  $0.052$  in  $C_p$  units.

comparing intensity ratio measurements at the pressure tap locations with the actual pressure tap data. This method is most convenient when, as was the case with the CRM model, accurate photogrammetry is available and a large number of pressure taps can be seen in all camera views. The PSP intensity ratio data were fitted to the corresponding tap data using a first order polynomial. A separate fit was generated for each image. A typical scatter plot of PSP vs pressure tap data following *in situ* calibration is shown in figure 8. The mean  $1-$

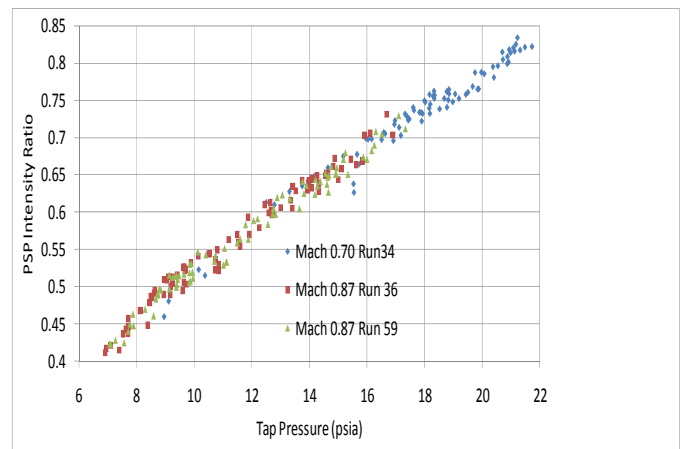


Figure 10 Scatter plot of PSP intensity ratio (prior to calibration) vs pressure taps for first run (34), first run at maximum Mach (36), and last run (58) in PSP data.

sigma scatter between tap and PSP data over the entire test was  $0.05 C_p$ . No significant trends were noted when plotting scatter data vs Mach,  $\alpha$ , camera, or configuration.

One question which naturally arises with *in situ* calibrations is to what degree the fit parameters vary with camera and condition over the course of the test. Such variation may indicate sensitivity to extraneous illumination or a calibration shift in the PSP. Figure 9 shows scatter plots for all four cameras at the same test condition. The difference between the fits calculated for the different cameras is within the scatter of the data indicating that, to the extent that can be determined from the data, all four cameras are demonstrating the same response to the pressure-sensitive paint. Figure 10 shows a similar comparison of scatter plots, but in this case for three runs taken at different tunnel conditions. (The tap data are shown as absolute pressures rather than pressure coefficient since  $C_p$  data would show an extraneous shift due to changes in static and dynamic pressure.) The PSP data follow the same calibration curve (to within the scatter of the data) over the full Mach range and over full span of the PSP data set. There is no detectable PSP calibration shift with time or tunnel condition during the CRM test.

*Image mapping:* Following calibration, PSP images from each camera were mapped to the model surface grid using the transformation from model to image coordinates developed by previously. Figure 11 shows the typical result of an image mapping operation. Data from all four cameras are combined onto a single grid. When a grid point is seen by more than one camera the mapping software chooses one camera to take data from. The choice is based on a “view quality” parameter derived from the obliquity with which the model surface is viewed and the local image magnification. If the obliquity is greater than  $70^\circ$  for all cameras, no data are mapped to that surface patch. For the present test, this only occurs at the fuselage nose, tailcone, and the leading edges of the wing and horizontal stabilizer.

### III. RESULTS AND DISCUSSION

This section presents a sample of the PSP data, beginning with the calibrated image data, and including some comparison with CFD results.

#### A. PSP Image Data

The PSP data are especially useful for illustrating the strong effect of Mach number and pitch angle on the flow over the wing upper surface. Figure 12 shows an overview of the wing upper surface data from camera 1 vs Mach and angle of attack for the WBT+2 configuration. At  $M = 0.70$  the surface pressure variation is dominated by the strong leading edge suction region which forms as  $\alpha$  increases from  $0^\circ$  to  $4^\circ$ . At higher Mach numbers the peak  $C_p$  is reduced but the suction region extends over a larger area. Shocks, absent at the lower Mach number, appear, and coalesce into a single strong shock at the highest  $\alpha$ . At all three Mach numbers the highest suction occurs nearest the wing root due presumably to the effect of washout.

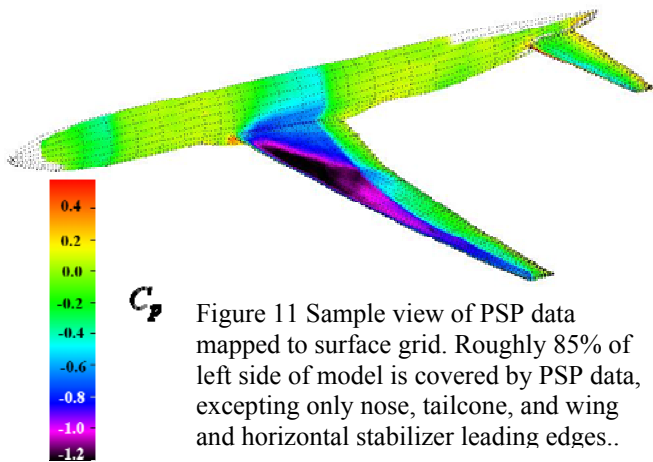


Figure 11 Sample view of PSP data mapped to surface grid. Roughly 85% of left side of model is covered by PSP data, excepting only nose, tail cone, and wing and horizontal stabilizer leading edges..

One feature visible in the PSP data is the apparent effect of trip dots on the pressure distribution. This can be seen in figure 13, which shows close up views of the wing upper surface over a range of  $\alpha$ . At  $\alpha = 0^\circ$ , it can be seen that the suction peak has a sharply defined edge located at a constant chord. The sharp beginning of the suction peak occurs at 10% chord, coincident with the trip dots. At  $\alpha = 1^\circ$ , the suction peak leading edge has moved forward, but a sharp pressure change can still be seen at 10% chord. At the inboard and outboard wing sections the appearance is of an initial peak, followed by drop in suction, followed by a second peak at 10% chord. The effect persists at higher angles of attack, but is confined to the inboard and outboard ends of the wing. The behavior of the pressure distribution can also be seen in cuts through the PSP data along chordwise lines. Figure 14 shows line cuts through the data in figure 13, at the spanwise locations marked by dark lines in the figure. Initially (at  $\alpha = 0^\circ$ ) a very sharp suction peak can be seen beginning at 10% chord. At  $\alpha = 1^\circ$  there appears to be a smaller suction peak ahead of the main peak, separated by a suction drop at 10% chord. At  $\alpha = 2^\circ$  the two suction peaks

have equal strength, and at  $\alpha = 4^\circ$  the appearance of a sharp feature at 10% chord has been lost.

This suction peak feature occurs in the wing upper surface data for all three configurations, but never on the lower surface. It can be seen to a lesser degree in some cases in the suction surface data for the horizontal stabilizers.

#### B. PSP/CFD Comparison

Mapping of PSP data to the CFD grid allows a direct comparison between the two data sources. However at this point comparisons between PSP and CFD are at a preliminary stage, and only some very limited comments can be made. Sclafani<sup>23</sup> *et. al.*, in their report on CFD predictions for the CRM have supplied some pressure data for the WBT0 configuration at an angle-of-attack corresponding to a lift coefficient of 0.5. (Reference 23, figure 36). This configuration and lift coefficient appears to correspond most closely to Run 57, Seq 7 of the PSP data set (WBT0,  $M = 0.85$ ,  $\alpha = 3^\circ$ ), however additional work is necessary to verify that the test conditions are the same. With this proviso, the PSP data shown in figure 13 cover the same chordwise cuts, at  $\eta = 28.3\%$  and  $\eta = 72.7\%$ , corresponding to the results shown by Sclafani.

The PSP data at  $\eta = 28.3\%$  show the same shock location at the CFD results, at roughly 60% chord, but the show a higher suction peak. Additionally the CFD suction peak has a sharper onset (occurs closer to the leading edge) than the PSP suction peak. The lower surface PSP and CFD data appear identical to within the resolution of the PSP data. At  $\eta = 72.7\%$  the PSP data appears to put the shock location slightly forward of that shown by the CFD. The PSP resolution is not sufficient to capture the slight recovery after the shock shown in the CFD results, and the PSP data also report a higher pressure downstream of the shock. The PSP also reports higher pressures on the lower surface.

### IV. CONCLUDING REMARKS

Pressure-sensitive paint data have been obtained over the left side of the CRM model at three configurations, for three transonic Mach numbers and nine angles of attack. The data were obtained with a four-camera PSP system using the luminescence lifetime approach. The camera and lamp setup was designed using virtual imaging software. This allowed the setup to a) to maximize the viewable model area, b) ensure good views of pressure taps from each camera to simplify *in situ* calibration, c) optimize PSP lighting, d) minimize interference with other instruments. The test was conducted at high Reynolds numbers which resulted in shorter PSP luminescence lifetime and lower paint brightness at the test condition, relative to standard PSP tests in the 11ft. This was counteracted by using shorter camera gate and flash times, and also by using new high brightness LED lamps. The result was shorter exposure times and fewer accumulations per image despite the lower paint brightness.

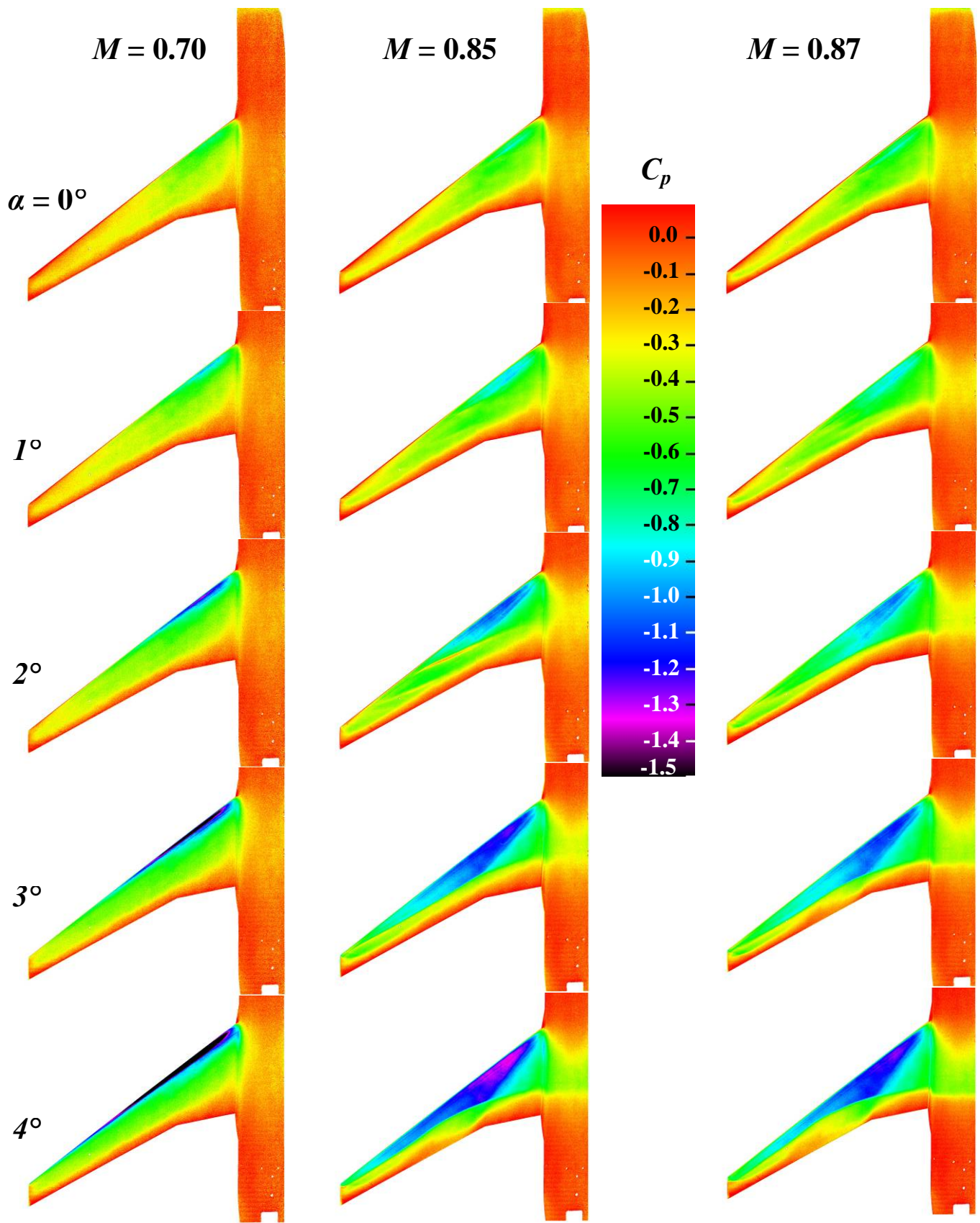


Figure 10 Wing upper surface images at showing variation of pressure with Mach and  $\alpha$  for WBT+2 configuration.



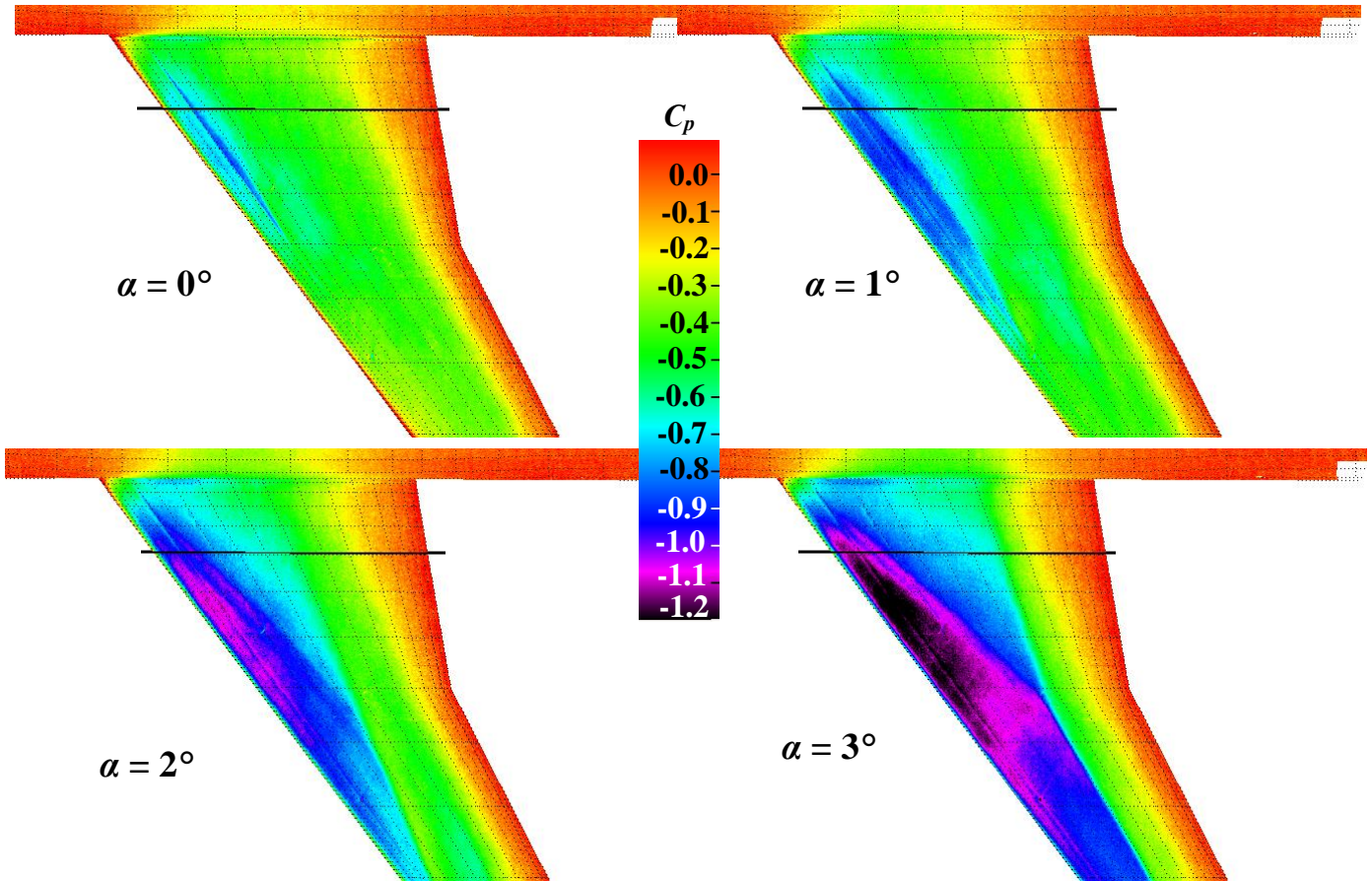


Figure 11 Wing upper surface images at  $M=0.85$ ,  $\alpha=0^\circ$ ,  $1^\circ$ ,  $2^\circ$ , and  $3^\circ$  for WBT0 configuration. (Run 57) PSP data are texture-mapped to CFD grid and model grid lines are shown. Horizontal black lines mark position of line cuts shown in figure 12. Abrupt rise in suction follows line of trip dots at 10% chord.

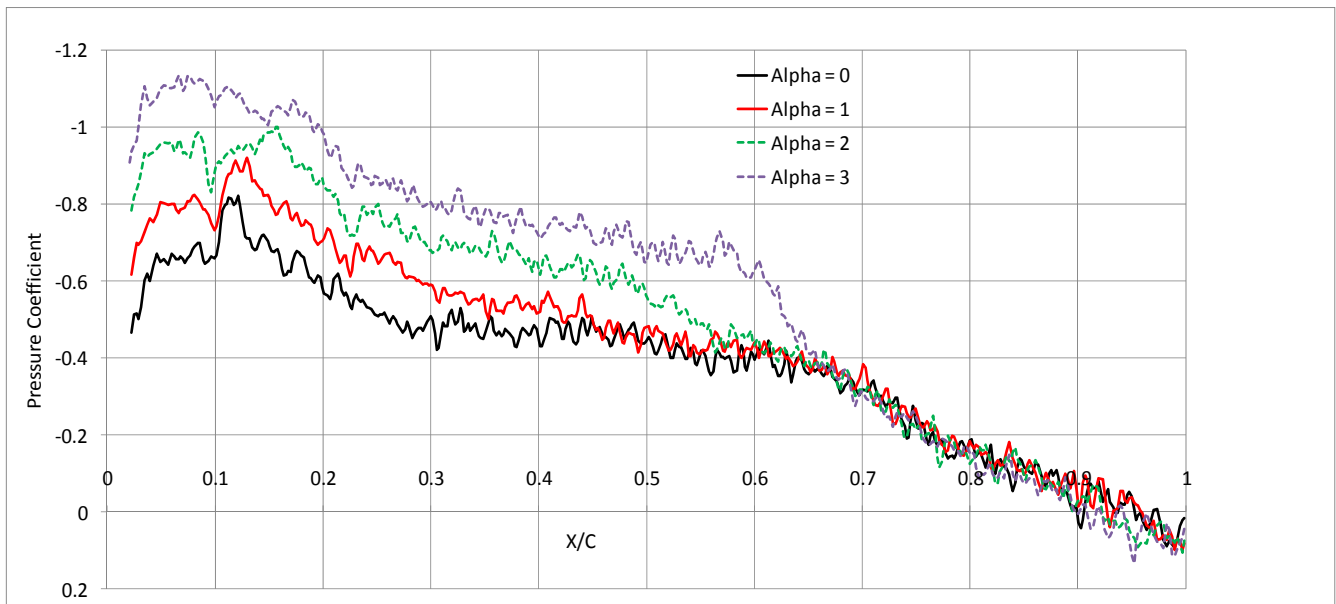


Figure 12. Line cuts through wing upper surface PSP data at locations shown in figure 11.



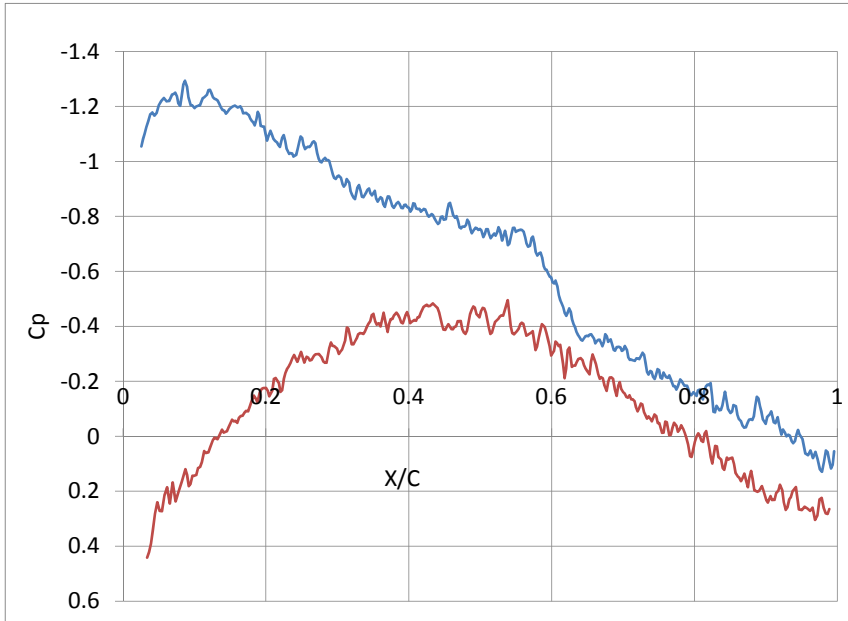


Fig 13(a). PSP data for WBT0,  $M = 0.85$ ,  $\alpha = 3^\circ$ ,  $\eta = 28.3^\circ$ .

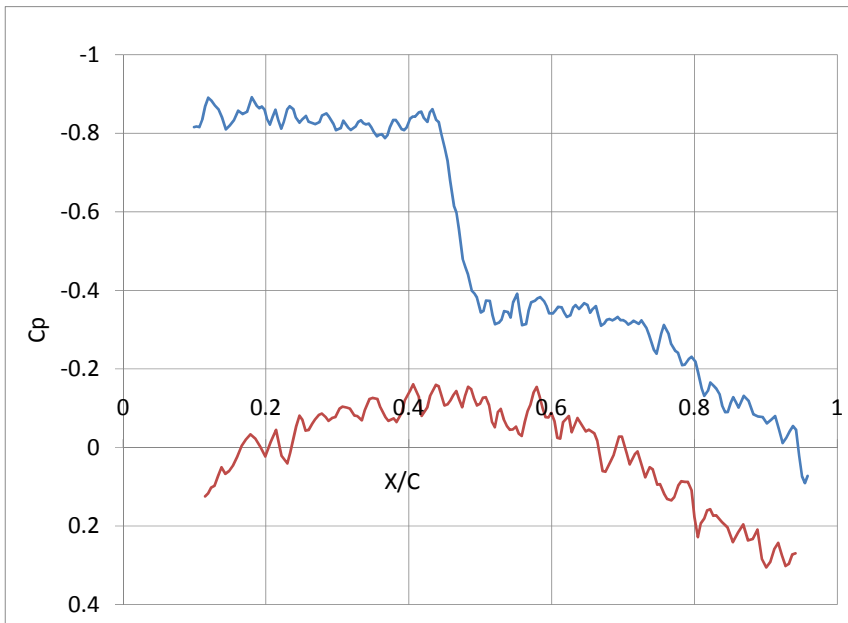


Fig 13(a). PSP data for WBT0,  $M = 0.85$ ,  $\alpha = 3^\circ$ ,  $\eta = 72.7^\circ$ .

The model was prepared and painted outside of the test section, minimizing occupancy costs associated with PSP. Target dot application used a new technique which made target dot locations available for other experimental techniques as well as PSP. Paint was applied to the entire model to ensure a uniform surface finish, and the paint was annealed prior to installation of the model in the tunnel.

PSP data were acquired semi-automatically, with the operator choosing camera exposure times before the start of the run, while data acquisition during each run was controlled by the wind tunnel data system. Data were reduced using wind-off reference images for correction of variation in the paint intrinsic lifetime. *In situ* calibration was used to fit the PSP intensity ratio data to the pressure tap data for each image separately. No calibration drift was observed either from camera to camera or throughout the course of the test. Scatter between PSP and pressure tap measurements was 0.05 in  $C_p$  units over the test. No consistent variation of scatter with test conditions (Mach,  $\alpha$ , etc.) was observed. Reduced PSP data were mapped onto the CFD surface grid.

The wing upper surface data consistently show a sharp increase in suction at 10% chord, coincident with the pressure tap locations. This behavior does not occur on the lower surface or the upper surface at low Mach number, suggesting that it is due to a flow feature rather than a spurious signal from the PSP. Other, unpublished, PSP data on transonic wings also show this behavior.

Comparison of PSP and CFD data is in a preliminary state. Differences are seen between the present PSP data and published CFD data for the CRM. However until PSP and CFD test conditions can be reviewed for consistency, no conclusions can be drawn.

#### ACKNOWLEDGMENTS

The successful accomplishment of the test objectives was made possible only by the tireless efforts of Louise Walker, Laura Kushner, and Barry Porter in the setup and operation of the PSP system.

#### REFERENCES

---

<sup>1</sup> Wahls R, Rivers M, Vasberg J, DeHaan M, 2008, Development of a Common Research Model for Applied CFD Validation Studies, AIAA 2008-6919, Presented at the AIAA Applied Aerodynamics Conference, Honolulu, HI, 20 August 2008

<sup>2</sup> Rivers MB, Dittberner A 2010 Experimental Investigation of the NASA Common Research Model AIAA 2010-4218, Presented at the 28<sup>th</sup> AIAA Applied Aerodynamics Conference, Chicago IL, 28 June – 1 July 2010

<sup>3</sup> Liu T, Campbell BT, Burns SP, Sullivan JP. 1997 Temperature- and Pressure-Sensitive Luminescent Paints in Aerodynamics, *Appl. Mech. Rev.*, vol. 50, no. 4, April

<sup>4</sup> Bell JH, Schairer ET, Hand LA, Mehta RD. 2001 Surface Pressure Measurements Using Luminescent Coatings. In *Annu. Rev. Fluid Mech.*, vol. 33, pp. 155-206.

---

<sup>5</sup> Crites R, Benne M. 1995 Emerging Technology for Pressure Measurements in Wind Tunnels – Pressure Sensitive Paint, AIAA 95-0106, Presented at the 33rd Aerospace Sciences Meeting, Reno NV, Jan 9-12

<sup>6</sup> Schanze K, Carroll B, Korotkevitch S, Morris M 1997 Concerning the Temperature Dependence of Pressure Sensitive Paints, AIAA 97-0386, Presented at the 33rd Aerospace Sciences Meeting, Reno NV, Jan 6-10

<sup>7</sup> Bell JH, 2001 Accuracy Limitation of Lifetime-Based Pressure Sensitive Paint Measurements. 19th International Congress on Instrumentation in Aerospace Simulation Facilities, Cleveland, Ohio, August 27-30.

<sup>8</sup> Goss LP, Trump DD, Sarka B, Lydick LN, Baker WM, 2000 Multi-Dimensional Time-resolved Pressure-Sensitive-Paint Techniques: A Numerical and Experimental Comparison, AIAA-2000-0832, Presented at the 38th Aerospace Sciences Meeting, Reno NV, 10-13 Jan.

<sup>9</sup> Radchenko VN. 1985. Application of the luminescence in aerodynamic researches. Master's thesis. Moscow Phys.-Tech. Inst., Zhukovsky, Russia (In Russian)

<sup>10</sup> Levy R 1992 "Luminescence Lifetime Measurements", 2<sup>nd</sup> Pressure-Sensitive Paint Workshop, Hampton, VA

<sup>11</sup> Liu T, Torgerson SD, Sullivan JP, Johnston R, Fleeter S, 1997 Rotor Blade Pressure Measurement in a High Speed Axial Compressor using Pressure and Temperature Sensitive Paints AIAA-97-0162, Presented at the 35th Aerospace Sciences Meeting, Reno NV, 6-10 Jan.

<sup>12</sup> Davies AG, 1998 Temperature Compensated PSP Measurements on a 2D Wing in Transonic Flow, Presented at the 6<sup>th</sup> Pressure-Sensitive Paint Workshop, Seattle WA 6-8 Oct.

<sup>13</sup> Holmes J W 1998 Analysis of radiometric, lifetime and fluorescent lifetime imaging for pressure sensitive paint *Aeronaut. J.* **2306** 189–94 1157

<sup>14</sup> Lydick LN 1999 Keynote Address, Presented at the 7<sup>th</sup> Pressure-Sensitive Paint Workshop Purdue IL 11-13 Oct.

<sup>15</sup> Baker WM 2001 Recent Experiences with Pressure Sensitive Paint Testing AIAA-2001-0306, Presented at the 39th Aerospace Sciences Meeting, Reno NV, 8-11 Jan.

<sup>16</sup> Sellers ME 2000 Application of Pressure Sensitive Paint for Determining Aerodynamic Loads on a Scale Model of the F-16C AIAA-2000-2528, Presented at the 21st Aerodynamic Measurement Technology and Ground Testing Conference Denver CO, 19-22 June.

<sup>17</sup> Amaya, M.A. & Kmak, A.R. (2002) "Capabilities of the NASA Ames Unitary Plan Wind Tunnel (UPWT)", Presented at the 40<sup>th</sup> Aerospace Sciences Meeting, Reno, Nevada, January 10-15.

<sup>18</sup> Amaya, M.A. & Boone, A.R. (2005) "Calibration of the 11-By 11-Foot Transonic Wind Tunnel at the NASA Ames Research Center", *AIAA Paper 2005-4277*, Presented at the 41st AIAA/ASME/SAE/ASEE Joint Propulsion Conference and Exhibit, Tucson, Arizona, July 10-13.

<sup>19</sup> AO (2005) "Test Planning Guide for High Speed Wind Tunnels", Revision 5, April 27, 2005. Document A027-9391-XB2, Prepared by the Technical Publications Group for The

---

Wind Tunnel Operations Division, Ames Research Center,  
Moffett Field, California

<sup>20</sup> Schairer, E. T.; Heineck, J. T.; Walker, S. M.; Yaste, D. M.;  
"Predicting Camera Views for Image-Based Measurements in  
Wind Tunnels," AIAA 2005-1349, 43rd AIAA Aerospace  
Sciences Meeting and Exhibit, 2005.

<sup>21</sup> Kushner, L. K.; Schairer, E. T.; "Planning Image-Based  
Measurements in Wind Tunnels by Virtual Imaging",  
AIAA Aerospace Sciences Meeting, Orlando, Florida, January  
3-8, 2011.

<sup>22</sup> Ponomarov S, Gouterman M 2000 Ideality of Pressure-  
Sensitive Paint, I. Platinum Tetra(penta-fluorophenyl)porphine  
in Fluoroacrylic Polymer, J. Appl. Polym. Sci. 77(13), 2795  
(2000)

<sup>23</sup> Sclafani AJ, DeHaan MA, Vassberg JC, Rumsey CL,  
Pulliam TH, 2010 Drag Prediction for the NASA CRM Wing-  
Body-Tail Using CFL3D and OVERFLOW on an Overset  
Mesh AIAA 2010-4219 28th AIAA Applied Aerodynamics  
Conference 28 June - 1 July 2010, Chicago, Illinois